Supplementary Information for

Boosting the Water Dissociation Kinetics via Charge Redistribution of Ruthenium Decorated on S, N-Codoped Carbon

Tingya Li,[a,#] Xueyan Zhang,[a,#] Yilan Chen,[a] Lixiang Zhong,[b] Shuzhou Li,[b] Peixin Zhang[a*] and Chenyang Zhao[a*]

[a] College of Chemistry and Environmental Engineering Shenzhen University Shenzhen 518071, China, E-mail: cyzhao@szu.edu.cn; pxzhang@szu.edu.cn.

[b] School of Materials Science and Engineering Nanyang Technological University 50 Nanyang Avenue 639798, Singapore

[#] Tingya Li and Xueyan Zhang contributed equally to this work.

Table of Contents

Experimental Procedures

Materials: Aniline (99.9%), thiophene (99%), ammonium persulphate ($(NH)_4S_2O_8$, 98%), $RuCl_3$ and KOH were purchased from Aladdin Reagents Ltd. Concentrated Hydrochloric acid, Pt/C (20 wt%) and Nafion (5 wt%) were purchased from Sigma-Aldrich. All the materials in the experimental were analytical grade and used without any further purification. The deionized water (DI) used throughout all experiments was purified through a Millipore system.

Synthesis of PANI/PTh: 5 mmol aniline and 5 mmol thiophene were slowly added into a 250 ml beaker containing 50 ml of ethanol and 50 ml of 1 M HCl. Then, 2 mmol $(NH)_4S_2O_8$ were added to initiate the reaction and the mixture was stirred for 12 h under room temperature. The resulting poly(aniline-thiophene) copolymer (PANI/PTh) was isolated from the suspension by centrifugation. It was washed with water several times and finally freeze-dried.

Synthesis of Ru-SNC: 20 mg $RuCl_3$ was first dissolved in 20 ml of ethanol. The PANI/PTh obtained above was then added and the solution was vigorously stirred for 12 h to allow for sufficient absorption of Ru^{3+} ions. The resulting mixture was isolated by centrifugation and freeze-dried. The black powder was thermally annealed at 800 ^oC for 3 h with a heating rate of 5 ^oC min^{-1} under N_2 atmosphere. The obtained sample was denoted Ru-SNC-2. For comparison, two additional samples with different Ru contents were also prepared using the same method with 10 and 30 mg of $RuCl_3$, which were denoted Ru-SNC-1 and Ru-SNC-3, respectively.

Synthesis of Ru/C: 16 mg $RuCl_3$ and 200 mg Ketjenblack were dissolved in 20 ml of ethanol and stirred for 12 h at room temperature to form a homogeneous solution. The mixture was isolated by centrifugation and then freeze-dried. The black powder was thermally annealed at 800 ^oC for 3 h using a heating rate of 5 ^oC min^{-1} under N_2 atmosphere. After naturally cooling down, the obtained sample was denoted Ru/C.

Sample digestion: 1 mg of sample was put into a 100 mL Teflon pressure digestion vessel. 20 mL aqua regia was then added. The vessels were closed and the samples were digested for 8 hour at 180 ^oC. The solutions were cooled down to room temperature prior to opening the vessels. After that, the solutions were diluted to 100 mL with DI water.

Characterization: The morphology of the Ru-SNC were examined by field emission scanning electron microscopy (FESEM, Carl Zeiss, US), transmission electron microscopy (TEM, Hitachi, Japan) and spherical aberration corrected Transmission Electron Microscope (ACTEM, FEI Titan

Cubed Themis G2 300, US). Elemental mapping was conducted on the energy-dispersive X-ray spectrometer (EDS) attached to the ACTEM. X-ray diffraction was carried out using Cu Kα radiation and scanned between 10 - 90^{o} with 4 steps s^{-1} (Bruker D8, Germany). X-ray photoelectron spectroscopy (XPS) was used to analyze the chemical state of the samples (K-Alpha, Thermo Scientific, UK). Raman spectra were performed with a Renishaw confocal spectrometer at 532 nm (inVia Reflex, UK). The inductively coupled plasma atomic emission spectroscopy (ICP-AES) was performed on Optima 2100DV (Perkin Elmer Ltd., USA). Fourier transform infrared (FT-IR) spectroscopy was performed using KBr pellets. (IR Affinity, Shimadzu, Japan).

XAFS measurements: The X-ray absorption find structure spectra (Ru K-edge) were collected at 1W1B station in Beijing Synchrotron Radiation Facility (BSRF). The storage rings of BSRF was operated at 2.5 GeV with an average current of 250 mA. Using Si(111) double-crystal monochromator, the data collection were carried out in transmission/fluorescence mode using ionization chamber. All spectra were collected in ambient conditions. The acquired EXAFS data were processed according to the standard procedures using the ATHENA module implemented in the IFEFFIT software packages. The k3-weighted EXAFS spectra were obtained by subtracting the post-edge background from the overall absorption and then normalizing with respect to the edge-jump step. Subsequently, k3-weighted χ(k) data of Ru K-edge were Fourier transformed to real (R) space using a hanning windows (dk =1.0 $Å^{-1}$) to separate the EXAFS contributions from different coordination shells. To obtain the quantitative structural parameters around central atoms, least-squares curve parameter fitting was performed using the ARTEMIS module of IFEFFIT software packages.

Electrochemical measurements: All the electrochemical measurements were carried out via a standard three-electrode cell system on CHI 760E electrochemical workstation, which includes a L-shape glassy carbon electrode (3 mm in diameter, GCE), a Pt wire counter electrode, and a Ag/AgCl reference electrode. 3 mg of the catalyst (Ru-SNC, Pt/C, Ru/C) was added into a mixed solution containing 500 μL DI water, 480 μL EtOH and 20 μL Nafion (5 wt%). After sonication for 30 min, 5 μL of the catalyst ink was dropped onto the surface of the pre-treated GCE. After being dried in air, the catalyst-coated electrode was used for electrochemical test with a catalyst loading of 0.21 mg cm^{-2}. N_2-saturated 1 M KOH was used as the electrolyte. The linear sweep voltammetry (LSV) curves were obtained by sweeping between -0.2 and 0.11 V (*vs*. RHE) with a scan speed of 5 mV

s^{-1}. All the LSV curves were iR-corrected. The stability tests were performed at a scan rate of 100 mV s^{-1} for 5000 cycles. A Chronopotentiometric test was also conducted at 10 mA cm^{-2} for 100 h. Electrochemical impedance spectroscopy (EIS) was measured from 100 KHz to 0.1 Hz with an AC amplitude of 5 mV at the potential of -0.03 V (*vs.* RHE).

CO stripping test: The working electrode was immersed in deoxygenated 0.1 M $HClO_4$ and the cell was sealed with parafilm. CO was then bubbled into the electrolyte for 15 min. The potential of the electrode was set at 0.125 V. After that, the CO flow was switched to Ar for another 20 min to remove the residual CO. The CV was scanned at a rate of 20 mV s^{-1}.

Potential calibration: The reference electrode (Ag/AgCl) was calibrated to reversible hydrogen electrode (RHE) by testing CV in a highly pure H_2-saturated KOH solution (1.0 M) with a Pt wire and Pt plate as working and counter electrode at a scan rate of 10 mV s^{-1}. The average of potentials at which the current was zero was regarded as the thermodynamic potential for hydrogen evolution reaction (HER), which is -1.009 V in 1 M KOH (Figure S1). Therefore, the potential with respect to RHE in the experiments are all calculated as follows:

$$E\,(RHE) = E\,(Ag/AgCl) + 1.009$$

The calculation of turnover frequency (TOF): The HER turnover frequency is defined as the total hydrogen turnovers divided by total active sites on a certain geometric electrode area. The hydrogen turnovers can be obtained from hydrogen evolution current density under a certain overpotential, while the number of active sites of Pt/C and Ru-SNC can be calculated by CO stripping or Cu-underpotential deposition (UPD)[1]. The UPD is a phenomenon of Cu electrodeposition at a potential less negative than its equilibrium (Nernst) potential. The tests were carried out in a 0.1 M H_2SO_4 solution with/without 2 mM of $CuSO_4$. Under the above specified conditions, the Nernst potential of E (Cu^{2+}/Cu) is 0.242 V vs. RHE. First, the catalyst was cycled between 0.05-1.0 V for Pt/C and 0.05-0.8 V for Ru-SNC in the absence of $CuSO_4$ to use as the background. The scan was ended at 0.05 V to avoid any oxidation of the catalyst. The electrolyte was then changed to 0.1 M H_2SO_4 with 2 mM $CuSO_4$. The working electrode was held at 0.3 V (vs. RHE) for 100 s to ensure the complete formation of the atomic UPD layer while at the same time avoiding any bulk deposition of Cu, followed by a positive scan at a scan rate of 10 mV s^{-1}. The number of active sites can be calculated from the Cu stripping charge by subtracting the background determined in 0.1 M H_2SO_4 solution, assuming each Cu atom was absorbed on one active site. The final simplified equation can

be expressed as

$$TOF(S^{-1}) = \frac{i}{Q_{Cu}}$$

where i is the measured current (A) under a certain overpotential and Q_{Cu} is the net Cu stripping charge. For the CO stripping method, the number of active sites can be calculated from the CO stripping charge. The TOF can be calculated using the equation above, assuming each CO molecule was absorbed on one active site.

Computational details: Ab initio molecular dynamics (AIMD) simulations were utilized to study the phase transformation from crystalline Ru to amorphous cluster and the room temperature relaxation of one layer graphene with nitrogen and sulphur dopants using CP2K quantum chemistry and solid-state physics software package. For the latter system, Ru atoms were added to randomly form chemical bonds with nitrogen, sulphur, and carbon atoms. The basis set employed is hybrid gaussian and plane wave basis set (GPW)[2], and the basis set used in these AIMD simulations was MOLOPT_DZVP[3,4], with the cut-off energy of plane wave set to be 350 Ry. The exchange-correlation contributions were treated by generalized gradient approximation (GGA), the Perdew–Burke–Ernzerhof (PBE) functional. The DFT-D3 method with Becke-Jonson damping was adopted to account for long range dispersion effect with a cut-off radius of 26 Å. The relaxed structures were obtained via running AIMD under NVT ensemble (300K) for 20.0 picosecond (20000 steps with 1.0 femtosecond time step).

Density functional theory (DFT) simulations were used to evaluate the HER evolution process inside a superlattice using CP2K package. For $Ru_{16}SN$, the nanostructure morphologies achieved from AIMD simulations were optimized by LBFGS algorithm. The lattice parameters of the supercell were 19.7 Å, 17.1 Å, 34.7 Å, 90°, 90°, 90°. For $Ru_1S_1N_1$, the nanostructure with size 15Å×15Å was cut-off from AIMD relaxed 2D graphene substrate with edge carbon atoms hydrogenated. The lattice parameters of the supercell were 30 Å, 30 Å, 30 Å, 90°, 90°, 90°. The single Gamma point (1×1×1) was used. The convergence criteria were 5×10^{-7} tolerance of the charge density residual for electronic steps and 5×10^{-4} Hartree/Bohr in ionic relaxation force for ionic steps. After optimization, the cut-off energy of plane wave set was increase to 500 Ry for all structure to perform self-consistent DFT simulations. All electronic information such as electronic total energy, density of states was then extracted from self-consistent simulation results. Bader analysis[5] was used

to calculate charge transfers between Ru and graphene substrate after each self-consistent simulation.

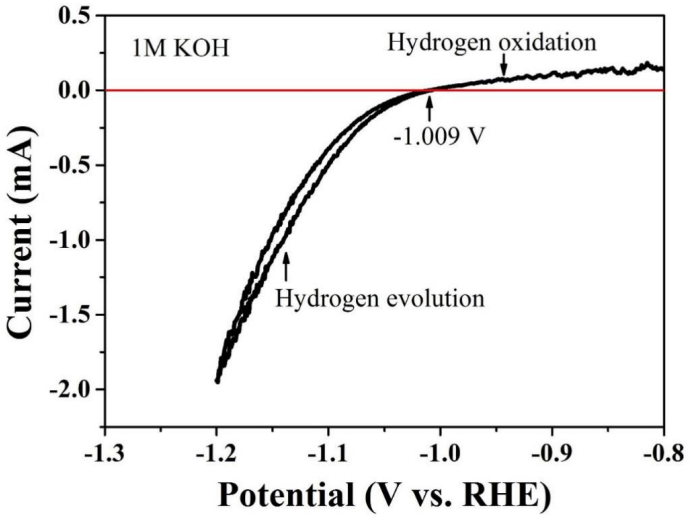

Figure S1. The calibrated potential of the Ag/AgCl reference electrode in 1 M KOH.

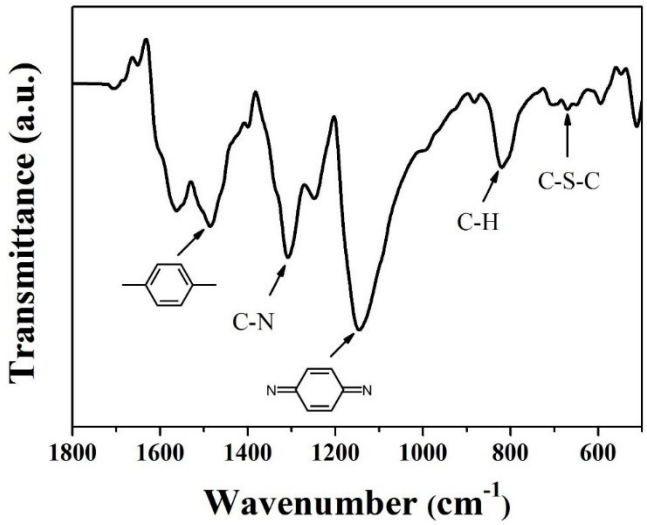

Figure S2. FT-IR spectrum of the PANI/PTh. The main bands at 1485 cm^{-1} and 1145 cm^{-1} correspond to the ring-stretching vibrations of the benzenoid and quinoid ring. The band at 1310 cm^{-1} with medium intensity is associated with C-N stretching vibration. The absorption peak centered at 671 cm^{-1} is attributed to the C-S-C stretching of the thiophene ring, while the peak centered at 820 cm^{-1} is due to the C-H out of plane vibration of the 2-5-substituted thiophene ring. Therefore, the FTIR results show the successful synthesis of PANI/PTh.

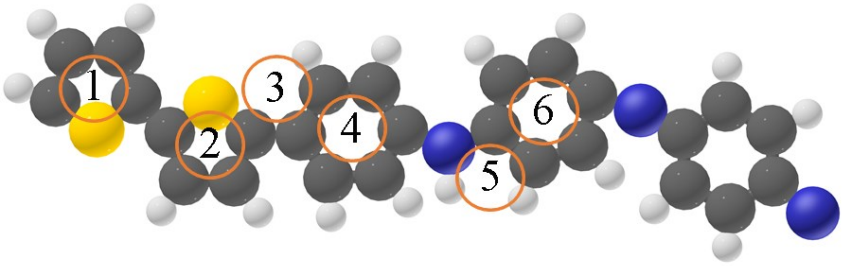

	1	2	3	4	5	6
E_{ads} (eV)	-4.094	-4.390	-3.814	-4.727	-3.137	-4.412

Figure S3. The absorption energy of Ru^{3+} ion on different sites of PANI/PTh. The C, N, S, and H atoms are represented by grey, blue, orange, and white spheres, respectively.

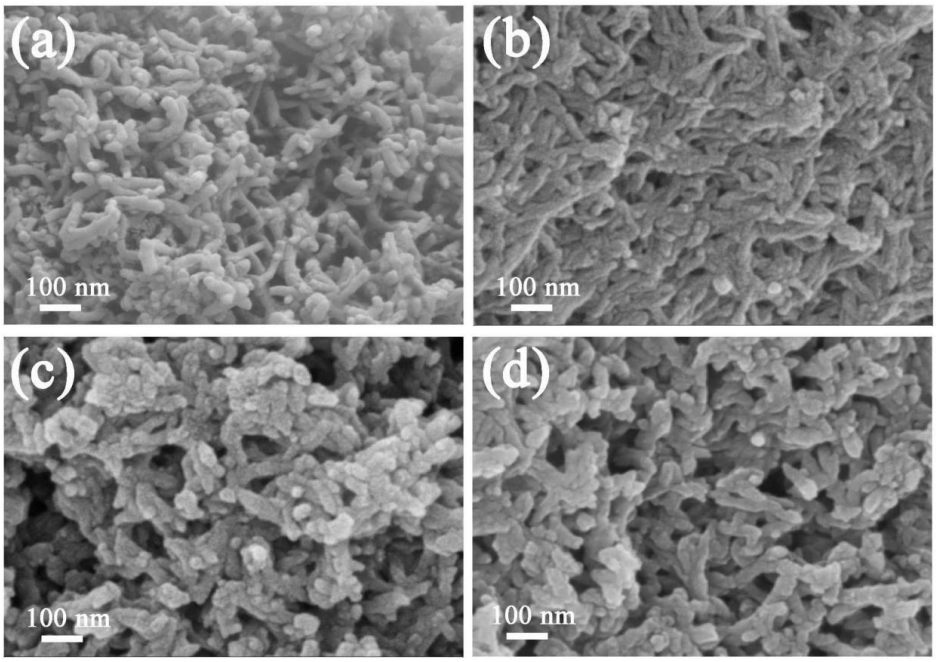

Figure S4. SEM images of (a) PANI/PTh, (b) Ru-SNC-1, (c) Ru-SNC-2 and (d) Ru-SNC-3, respectively.

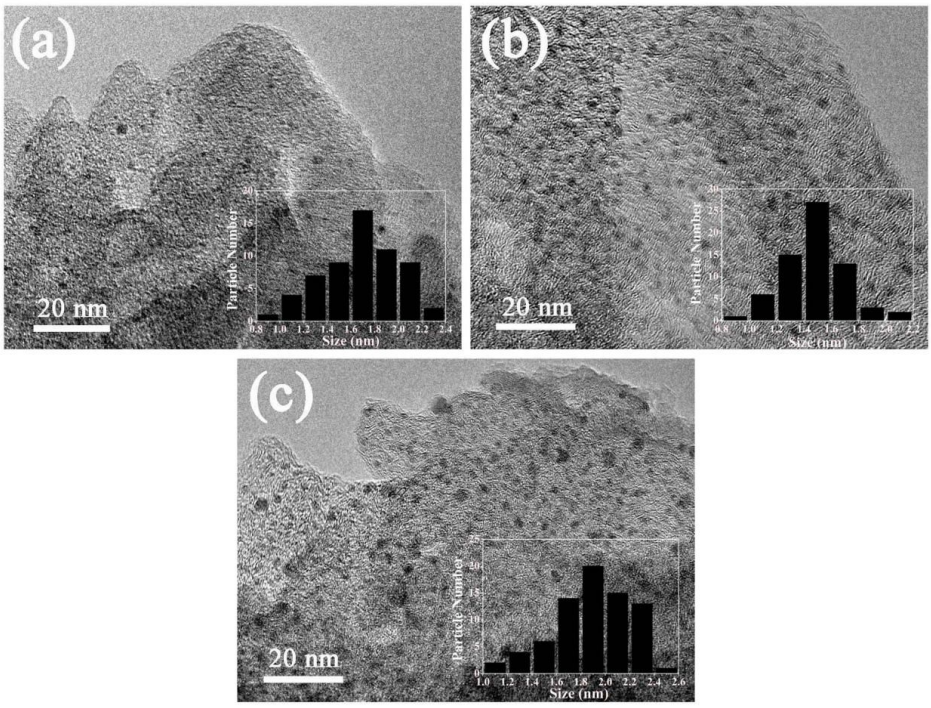

Figure S5. TEM images of (a) Ru-SNC-1, (b) Ru-SNC-2 and (c) Ru-SNC-3, respectively.

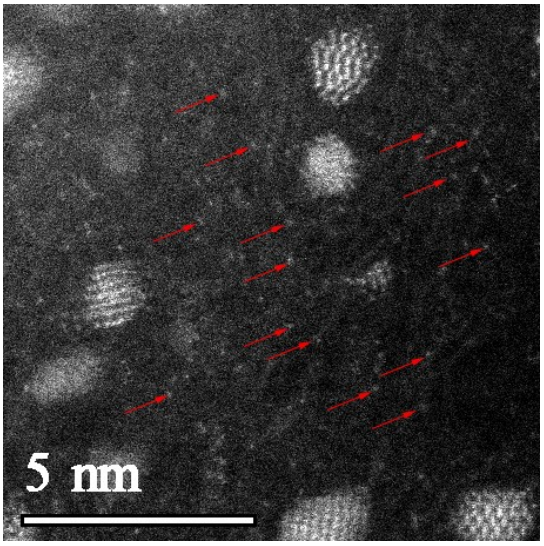

Figure S6. High-resolution aberration-corrected TEM image at different region of Ru-SNC-2.

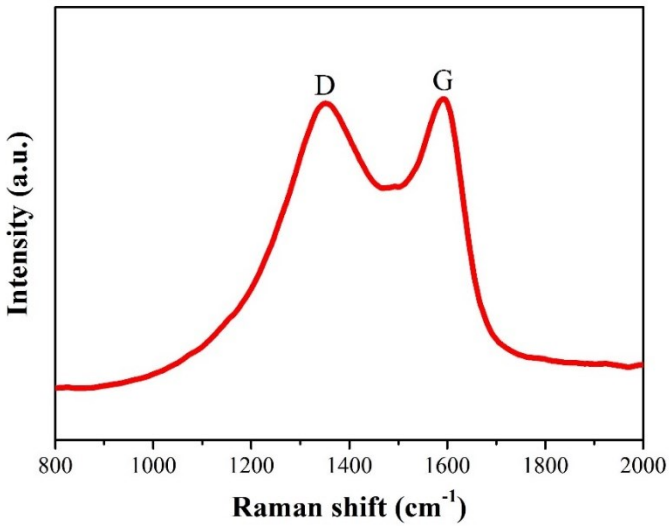

Figure S7. Raman spectrum of Ru-SNC-2. The D-band and G-band of carbon are located at 1350 and 1593 cm^{-1} with an I_D/I_G ratio of 0.92.

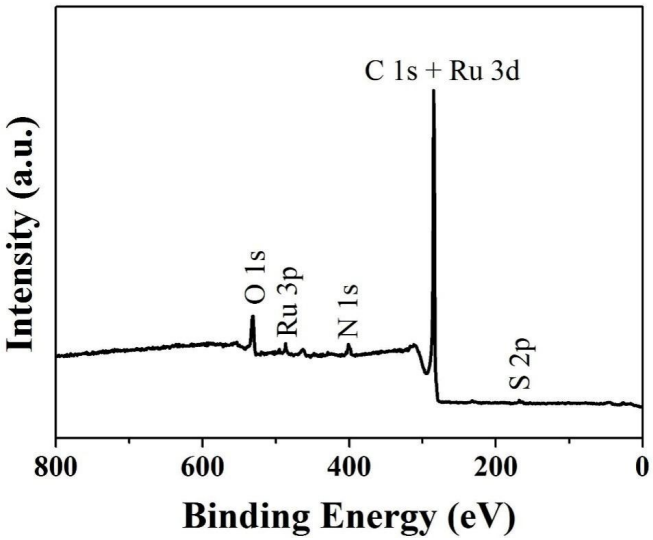

Figure S8. XPS survey spectrum of Ru-SNC-2. The enhanced signal of oxygen may be ascribed to the substrate and physically adsorbed trace water.

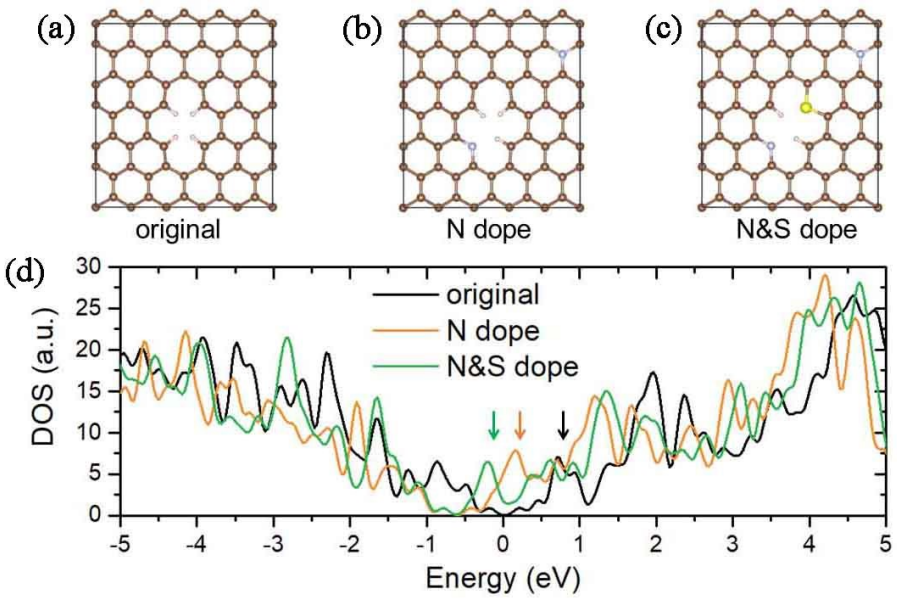

Figure S9. Possible structure representations of (a) original graphene, (b) N doped graphene, (c) N and S codoped graphene and (d) their corresponding density of states (DOS). The DOS results indicate that the N and S doping leads to enhanced electrical conductivity and alters the surface electronic distribution of carbon.

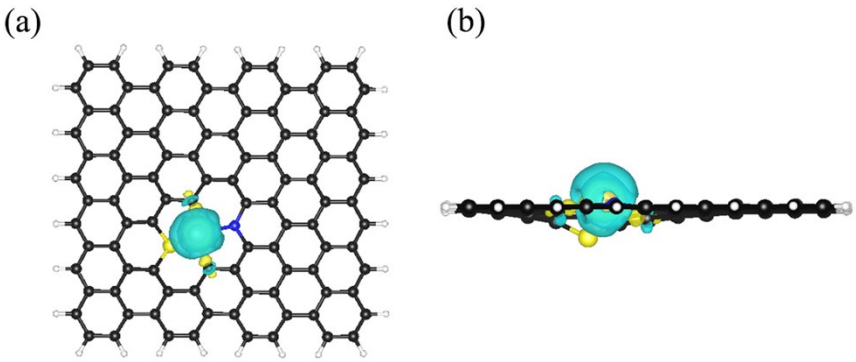

Figure S10. The (a) top and (b) side view of the charge difference of the Ru SA. The yellow and cyan regions refer to increased and decreased charge distributions, respectively.

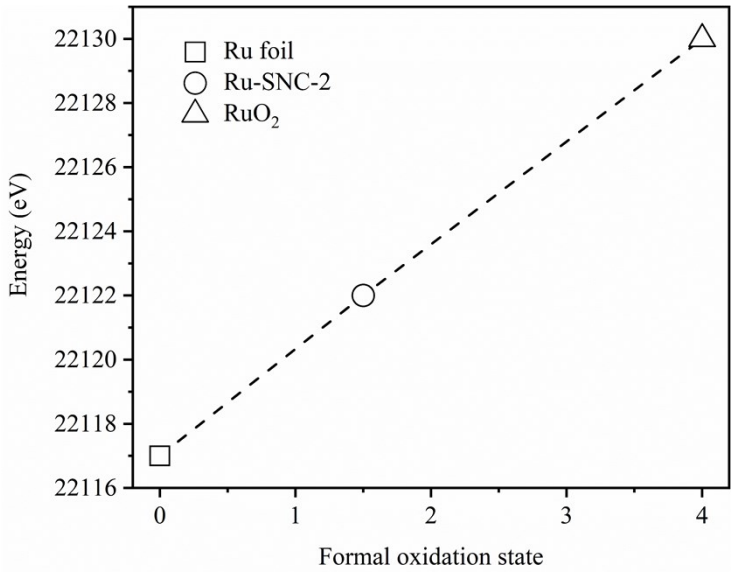

Figure S11. Correlation plot of the absorption Ru K-edge position for Ru foil, Ru-SNC-2 and RuO_2.

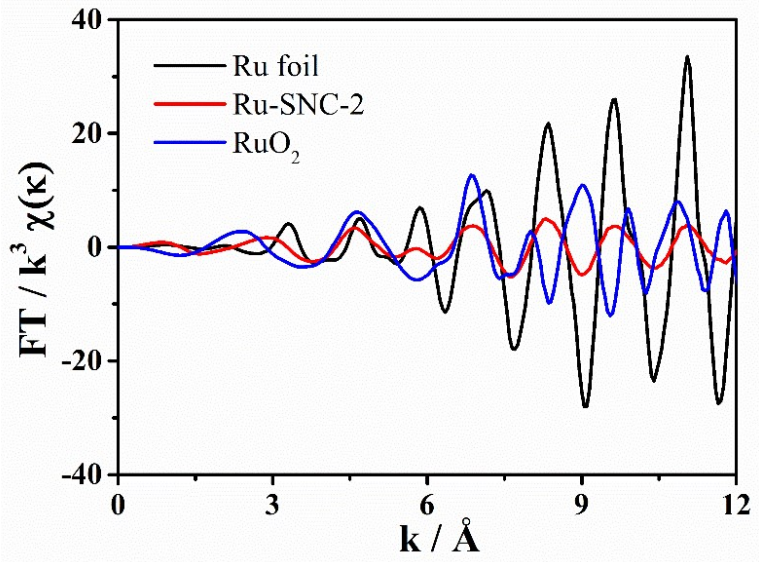

Figure S12. The Ru K-edge extended XANES oscillation functions of Ru-SNC-2, RuO_2 and Ru foil.

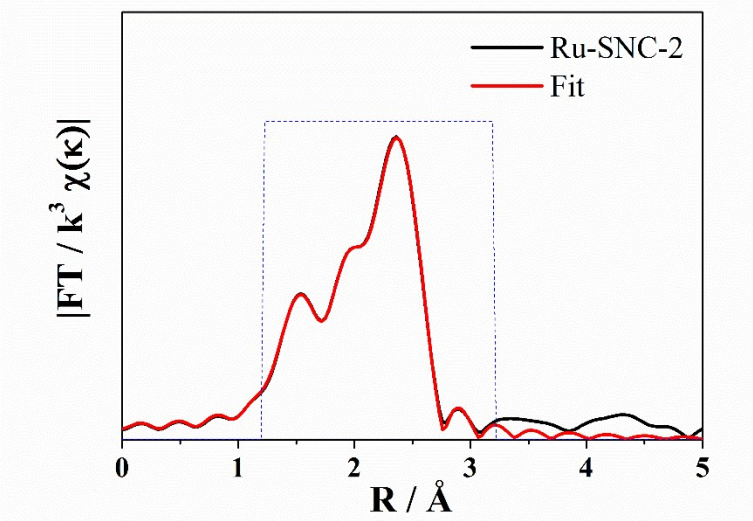

Figure S13. The best fitting curve for the Fourier transformed Ru K-edge EXAFS of Ru-SNC-2.

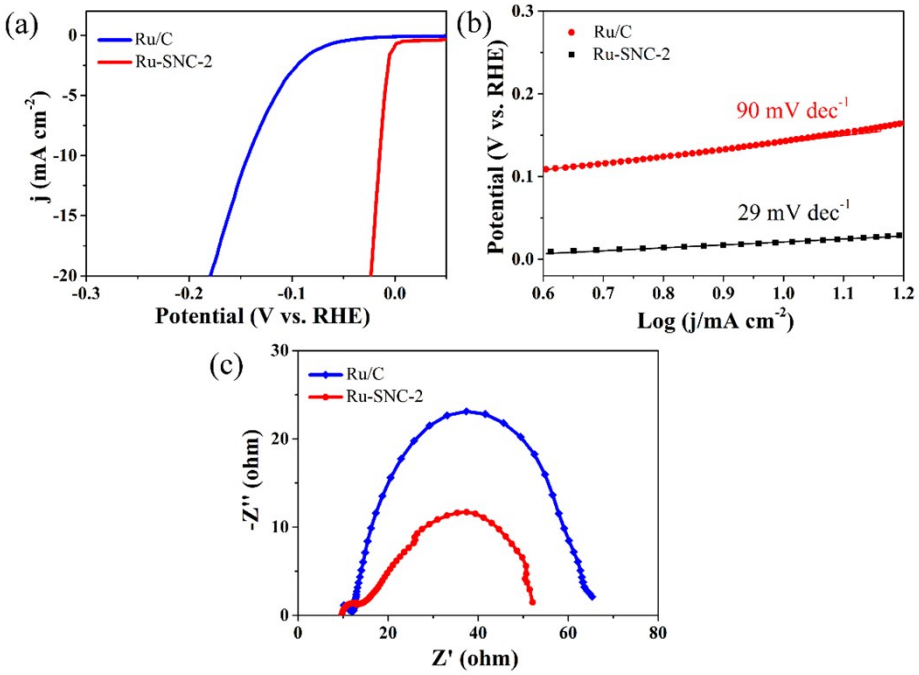

Figure S14. Ru-SNC-2 and Ru/C (a) LSV curve, (b) Tafel plot, (c) Nyquist plot at overpotential of 30 mV.

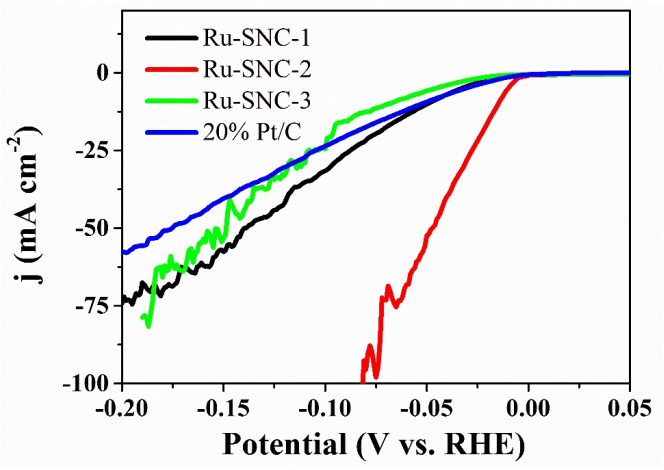

Figure S15. The LSV curves of the Ru-SNC and Pt/C at large current densities. Servious fluctuation were observed for all the samples as a result of the genetation and desorption of the H_2 bubbles.

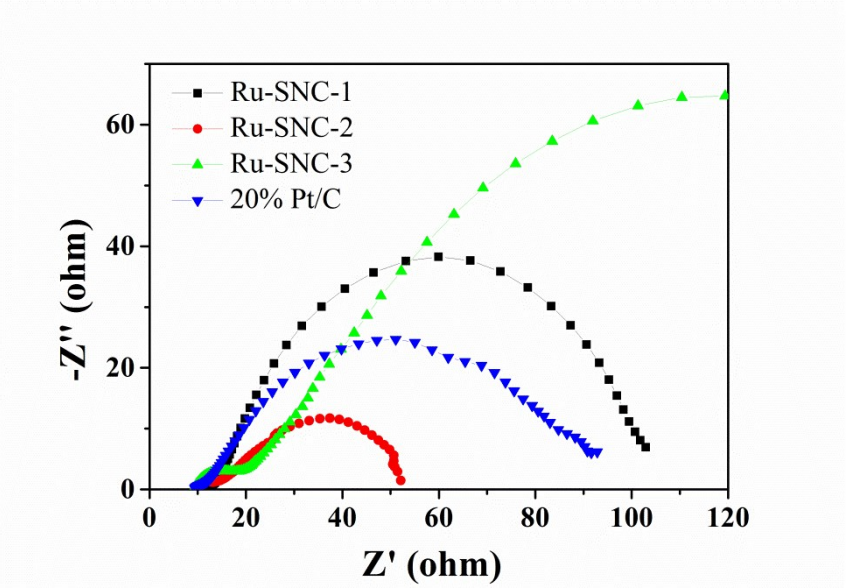

Figure S16. Nyquist plots of the Ru-SNC and 20% Pt/C.

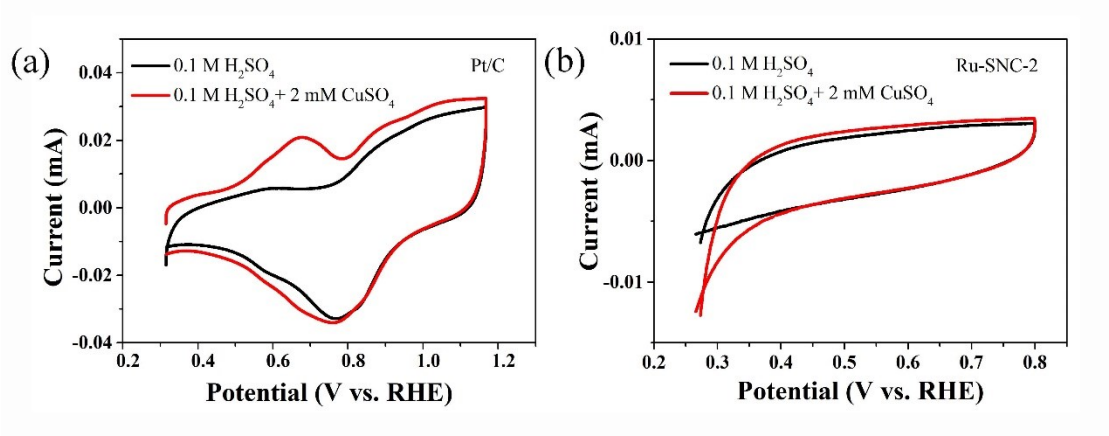

Figure S17. Determination of the active site number of (a) Pt/C and (b) Ru-SNC-2 by Cu-UPD method. The working electrode was held at 0.3 V (vs. RHE) for 100 s to ensure the complete formation of the atomic layer of Cu, while at the same time avoiding any bulk deposition of Cu, followed by a positive scan at a scan rate of 10 mV s^{-1}.

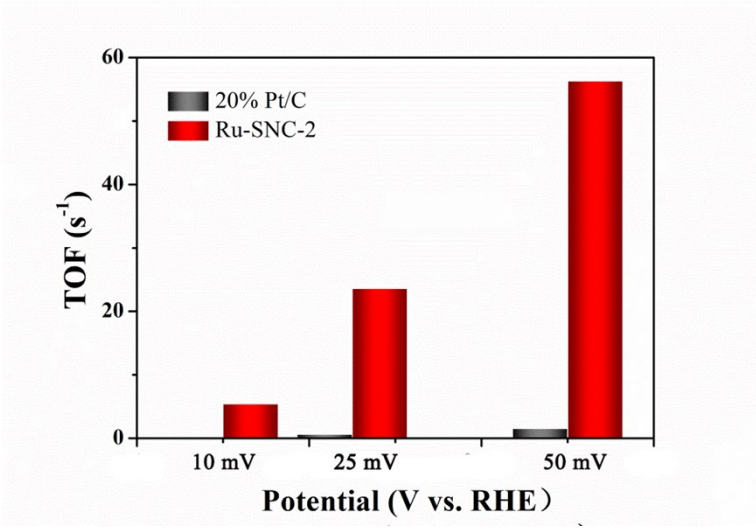

Figure S18. TOF values of Ru-SNC-2 and 20% Pt/C calculated from the CO-stripping at overpotentials of 10, 25 and 50 mV, respectively.

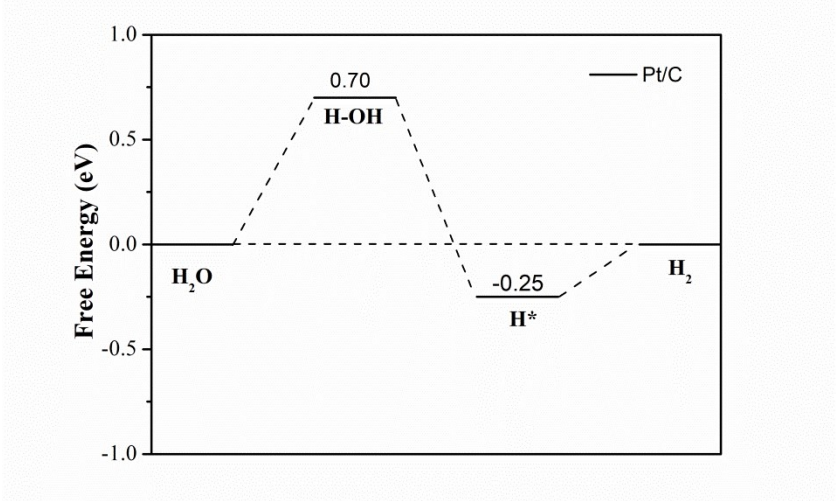

Figure S19. Calculated Gibbs free energy diagrams of Pt/C.

Table S1. EXAFS fitting parameters at the Ru K-edge for Ru-SNC-2.

Shell	N [a]	R (Å) [b]	σ^2 (Å^2·10^{-3}) [c]	ΔE_0 (eV) [d]	*R* factor (%)
Ru-N	1.0	1.95	2.9	-4.3	
Ru-S	0.8	2.29	3.0	2.9	0.2
Ru-Ru	4.0	2.67	7.6	-1.4	

[a] *N*: coordination numbers;

[b] *R*: bond distance;

[c] σ^2: Debye-Waller factors;

[d] ΔE_0: the inner potential correction.

R factor: goodness of fit. *S*02 was set as 0.90/0.90/0.835 for Ru-N/Ru-S/Ru-Ru, which was obtained from the experimental EXAFS fit of reference RuO_2 by fixing CN as the known crystallographic value and was fixed to all the samples.

Table S2. Comparison of state-of-the art electrocatalysts for alkaline HER.

Catalysts	Loading (mg cm^{-2})	Electrolytes	Overpotentials at 10mA cm^{-2} (mV)	Tafel plots (mV dec^{-1})	References
Ru-SNC-2	**0.21**	**1.0M KOH**	**14**	**29**	**This work**
Ru@NC	0.2	1.0M KOH	26	36	6
Ru@C_2N	0.285	1.0M KOH	17	38	7
RuP_2@NPC	1.0	1.0M KOH	52	69	8
RuCoP	0.3	1.0M KOH	23	37	9
Rh_2P	0.15	1.0M KOH	30	50	10
PtNi-O	0.005	1.0M KOH	39.8	41.7	11
Ru@GnP	0.25	1.0M KOH	22	28	12
CoP@BCN	0.4	1.0M KOH	122	59	13
$NiCo_2P_x$	5.9	1.0M KOH	58	34.3	14
NiS_2/MoS_2 HNW	0.2	1.0M KOH	204	65	15
Co/CoP	0.88	1.0M KOH	193	90	16
Ru-MoO_2	0.285	1.0M KOH	29	31	17

Table S3. The calculated energies for Pt), Ru (101), Ru-SA and Ru nanocluster at pH =14.

		Surface E (eV)	Molecule E (eV)	Total E (eV)	dE (eV)	dG (eV)
Pt 111	H_2O	-405.9812	-14.2314	-420.2126	0.0000	0.0000
	*H_2O			-419.5107	0.7019	0.7019
	*H		-409.8572	-409.8572	-0.4949	-0.2549
	0.5H_2	-405.9812	-6.7620	-409.3622	0.0000	0.0000
Ru 101	H_2O	-579.4735	-14.2314	-593.7049	0.0000	0.0000
	*H_2O			-593.2590	0.4459	0.4459
	*H		-583.6190	-583.6190	-0.7645	-0.5245
	0.5H_2	-579.4735	-6.7620	-582.8545	0.0000	0.0000
Ru	H_2O	-4870.5331	-14.2314	-4884.7645	0.0000	0.0000
nanocluster	*H_2O			-4884.4665	0.2980	0.2980
	*H		-4874.3493	-4874.3493	-0.4352	-0.1952
	0.5H_2	-4870.5331	-6.7620	-4873.9141	0.0000	0.0000
Ru-SA	H_2O	-1038.1588	-14.2338	-1052.3926	0.0000	0.0000
	*H_2O		molecule E	-1051.7312	0.6614	0.6614
	*H			-1041.8838	-0.3440	-0.1040
	0.5H_2	-1038.1588	-6.7620	-1041.5398	0.0000	0.0000

Reference

1 C. L. Green and A. Kucernak, *J. Phys. Chem. B*, 2002, **106**, 1036-1047.

2 G. Lippert, J. Hutter and M. Parrinello, *Mol. Phys.*, 1997, **92**, 477-487.

3 M. Krack and M. Parrinello, *Phys. Chem. Chem. Phys.*, 2000, **2**, 2105-2112.

4 J. VandeVondele and J. Hutter, *J. Chem. Phys.*, 2007, **127**, 114105.

5 G. Henkelman, A. Arnaldsson and H. Jónsson, *Comput. Mater. Sci.*, 2006, **36**, 354-360.

6 Z. L. Wang, K. J. Sun, J. Henzie, X. F. Hao, C. L. Li, T. Takei, Y. M. Kang and Y. Yamauchi, *Angew. Chem. Int. Ed.*, 2018, **57**, 5848-5852.

7 J. Mahmood, F. Li, S. M. Jung, M. S. Okyay, I. Ahmad, S. J. Kim, N. Park, H. Y. Jeong and J. B. Baek, *Nat. Nanotechnol.*, 2017, **12**, 441-446.

8 Z. H. Pu, I. S. Amiinu, Z. K. Kou, W. Q. Li and S. C. Mu, *Angew. Chem. Int. Ed.*, 2017, **56**, 11559-11722.

9 J. Y. Xu, T. F. Liu, J. J. Li, B. Li, Y. F. Liu, B. S. Zhang, D. H. Xiong, I. Amorim, W. Li and L. F. Liu, *Energy Environ. Sci.*, 2018, **11**, 1819-1827.

10 F. L. Yang, Y. M. Zhao, Y. S. Du, Y. T. Chen, G. Z. Cheng, S. L. Chen and W. Luo, *Adv. Energy Mater.*, 2018, **8**, 1703489.

11 Z. P. Zhao, H. T. Liu, W. P. Gao, W. Xue, Z. Y. Liu, J. Huang, X. Q. Pan and Y. Huang, *J. Am. Chem. Soc.*, 2018, **140**, 9046-9050.

12 F. Li, G. F. Han, H. J. Noh, I. Ahmad, I. Y. Jeon and J. B. Baek, *Adv. Mater.*, 2018, **30**, 1803676.

13 H. Tabassum, W. H. Guo, W. Meng, A. Mahmood, R. Zhao, Q. F. Wang and R. Q. Zou, *Adv. Energy Mater.*, 2017, **7**, 1601671.

14 R. Zhang, X. X. Wang, S. J. Yu, T. Wen, X. W. Zhu, F. X. Yang, X. N. Sun, X. K. Wang and W. P. Hu, *Adv. Mater.*, 2017, **29**, 1605502.

15 P. Y. Kuang, T. Tong, K. Fan and J. G. Yu, *ACS Catal.*, 2017, **7**, 6179-6187.

16 Z. H. Xue, H. Su, Q. Y. Yu, B. Zhang, H. H. Wang, X. H. Li and J. S. Chen, *Adv. Energy Mater.*, 2017, **7**, 1602355.

17 P. Jiang, Y. Yang, R. H. Shi, G. L. Xia, J. T. Chen, J. W. Su and Q. W. Chen, *J. Mater. Chem. A*, 2017, **5**, 5475-5485.